JOURNAL OF PROPULSION AND POWER
Vol. 24, No. 2, March–April 2008

Combustion of Boron–Titanium Nanocomposite Powders in Different Environments

Mikhaylo A. Trunov,* Vern K. Hoffmann,† Mirko Schoenitz,‡ and Edward L. Dreizin§
New Jersey Institute of Technology, Newark, New Jersey 07102

DOI: 10.2514/1.30483

Combustion characteristics were compared for aerosols of nanocomposite powders with the composition 2B + Ti, blended boron and titanium powders with the same bulk composition, and aluminum. Nanocomposite powders were prepared by arrested reactive milling. Experiments were conducted in a constant-volume explosion vessel filled with $N_2/O_2/CH_4$ mixtures, with volumetric oxygen concentration fixed at 22.5% and methane concentration varied from 0 to 12%. The flame temperature for aluminum powders remained close to 2560 K, whereas for the nanocomposite 2B + Ti, it increased from about 2180 to 2370 K as the methane concentration increased from 0 to 12%. Burn rates were consistently higher for the nanocomposite 2B + Ti powder, followed by aluminum and then by the blended 2B + Ti powder. The efficiency of combustion for all fuels was assessed by comparing the predicted and experimental portions of the combustion energy per unit mass of metal fuel used to produce the heated gaseous products. Nanocomposite 2B + Ti outperformed aluminum for all environments, with increasing difference in efficiency at higher methane concentrations. It was concluded that nanocomposite 2B + Ti powders enable one to achieve rapid and highly efficient combustion in both dry and wet gaseous environments.

Introduction

BORON has significant potential as a fuel additive because of its high gravimetric and volumetric combustion enthalpies [1,2]. However, its practical performance has been impeded by long ignition delays and formation of relatively stable HOBO compounds in water-containing oxidizing environments. The term HOBO describes a chemical structure H-O-B = O or HBO_2, a major reaction product in oxygen-rich B/O/H/C systems. HOBO was suggested to cause a kinetic bottleneck for the full oxidation of boron [1,3–5]. Heavier boron oxyhydrides (H_xBO_y, with x, $y > 2$) are important at relatively low temperatures (typically, below 1600 K) and are commonly excluded from the theoretical thermodynamic analysis of boron combustion occurring at much higher temperatures [5]. It has been suggested that extended ignition delays are caused by heterogeneous reactions at the interface between the boron particle and its surface oxide layer [6]. Alternative explanations (e.g., involving boron polymorphic phase changes affecting the diffusivity of boron atoms at specific temperatures) were also discussed in the literature [7].

Recently, several approaches to improve combustion of boron were proposed. One such approach is based on metastable nanocomposite materials, such as 2B + Ti or 2B + Zr, which are capable of highly exothermic metal–metalloid reactions, producing the respective borides (TiB_2 or ZrB_2). The materials comprise fully dense, micron-sized powders in which each particle represents a metal (Ti or Zr) matrix with nanosized boron inclusions. When initiated, the metal–metalloid reaction occurs rapidly over the entire metal–metalloid interface and heats the powder nearly adiabatically to a temperature at which full-fledged boron combustion begins. Thus, ignition delays are expected to be dramatically reduced, resulting in accelerated boron combustion. The feasibility of this approach was demonstrated in [8]. Very low ignition temperatures and complete combustion of the nanocomposite powders in air were achieved. However, the issue of the formation of HOBO compounds has not been addressed previously. This project aims to determine whether the accelerated burn rates and improved combustion efficiency demonstrated for nanocomposite Ti–B powders in air are maintained in water-containing environments. In addition, combustion rates and efficiencies of Ti–B nanocomposites and aluminum powders in the same set of environments are compared, with aluminum serving as a common reference. The composition 2B + Ti was chosen to derive the maximum energy release from the formation of TiB_2 ($\Delta H = -4.02$ kJ/g). The theoretical maximum density for the 2B + Ti composition is 3.51 g/cm^3, compared with 2.7 g/cm^3 for aluminum. Finally, the combustion enthalpy for an idealized reaction of $2B + Ti + 2.5O_2 \rightarrow TiO_2 + B_2O_3$ is −31.17 kJ/g, compared with −31.05 kJ/g for combustion of aluminum, considering a similarly idealized reaction $2Al + 1.5O_2 \rightarrow Al_2O_3$.

The combustion rate and completeness for nanocomposite samples and mixed powders with the same bulk composition of 2B + Ti, as well as for fine aluminum powder, were determined for dry and wet oxidizing environments. Powders were prepared using the recently developed technique of arrested reactive milling (ARM) [8–10]. Combustion experiments were performed using a constant-volume explosion technique [8,11–13]. The powders were ignited in systematically varied gas mixtures of air and methane. The powder loads were determined based on thermodynamic equilibrium calculations in which optimized fuel-to-oxidizer ratios were determined for each fuel and each environment. Combustion rates and flame temperatures were determined from the resulting pressure traces. Combustion completeness was assessed based on the phase analysis of condensed combustion products and from comparison between calculated and experimental flame temperatures.

Thermodynamic Calculations

Initial calculations were performed using the U.S. Air Force chemical equilibrium specific impulse (ISP) code and addressed combustion of Al and 2B + Ti in $O_2/N_2/CH_4$ gas mixtures. These calculations used a constant pressure close to that measured in

Presented as Paper 4809 at the 42nd AIAA/ASME/SAE/ASEE Joint Propulsion Conference and Exhibit, Sacramento, CA, 9–12 July 2006; received 16 February 2007; revision received 5 September 2007; accepted for publication 10 September 2007.

*Research Scientist, Department of Chemical Engineering. AIAA Member.
†Senior Research Engineer, Department of Chemical Engineering.
‡Assistant Research Professor, Department of Mechanical Engineering. AIAA Member.
§Professor, Department of Chemical Engineering. AIAA Senior Member.

experiments. In preliminary calculations, it was determined that changing the pressure in the range of 5–10 atm, covering the range of pressures observed in the experiments, results in a practically insignificant variation of the adiabatic flame temperature when condensed metal oxides are produced in combustion. Thus, calculations with the ISP code used a constant pressure of 6 atm. However, the experiments were performed in a constant-volume chamber, and a second series of thermodynamic calculations was later performed using the chemical equilibrium and applications (CEA) code by Gordon and McBride [14]. Calculations with the CEA code were performed at a constant volume of 9.2 liters, corresponding to the volume of the experimental explosion vessel. Several constant-pressure calculations performed using the CEA code for reference produced the same results as those obtained using the ISP code.

For both calculation series, the results need to be treated with caution. For example, for a constant-pressure calculation, the program considers the enthalpy change in an isobaric process and thus is expected to somewhat underestimate the temperature increase for a constant-volume experiment. The reaction pressures predicted by the constant-volume calculations significantly exceed the experimental pressures. Similarly, it is expected that the adiabatic reaction temperatures were substantially overpredicted by the constant-volume calculations when compared with the respective experiments, and thus the predicted reaction products could be substantially different from those produced in the experiments.

Despite the systematic errors, it is expected that the calculated adiabatic flame temperatures represent useful reference points. Furthermore, the trends for the adiabatic temperature as a function of the fuel type, gas composition, and equivalence ratio are representative of those expected in the experiments.

The calculations had two main objectives:

1) Determine the optimum metallic fuel loads for the constant-volume explosion experiments. Such loads are affected by the C–O and H–O reactions and are, therefore, different for different gas compositions. Charges were considered optimal when metal combustion resulted in the highest adiabatic flame temperature. In addition, it was desired that minor variations in the powder load resulting from experimental errors should not bias the recorded pressure significantly.

2) Establish adiabatic flame temperatures as benchmarks for the experimental combustion temperatures.

For both constant-pressure and constant-volume cases, two sets of calculations were performed. In the first set, the gas composition was varied systematically to increase the concentration of methane, whereas the concentrations of oxygen and metallic fuel remained constant. The volumetric concentration of oxygen was fixed at 22.5% of the gas mixture. The concentrations of metal fuels (i.e., Al or 2B + Ti) were fixed to represent the respective stoichiometric mixtures in the absence of any methane (as described by the preceding idealized combustion reactions); the fuel loads were the same for both constant-volume and constant-pressure calculations. An additional calculation with no metal fuel at all was conducted for each case to assess the expected temperatures (and pressures) of methane combustion. In the second set of calculations performed for several selected gas compositions, the amount of metal fuel was systematically varied, effectively changing the equivalence ratio. Three gas compositions, with 3, 6, and 12% of methane and with oxygen fixed at 22.5%, were considered.

The results of the first set of calculations are presented in Figs. 1 and 2. For the combustion of metal fuels in the $N_2/O_2/CH_4$ gas mixtures, the adiabatic flame temperature continuously decreases with increasing methane concentration, as shown in Fig. 1. This is not surprising, considering that both carbon and hydrogen compete for oxygen with metal, resulting in the overall decrease of the combustion enthalpy. The adiabatic combustion temperature of Al is consistently higher than that of 2B + Ti in both dry and wet environments. The predicted trends for the adiabatic flame temperature as a function of methane concentration for a fixed metal load are similar for the constant-volume and constant-pressure calculations. In both cases, the calculations for methane combustion

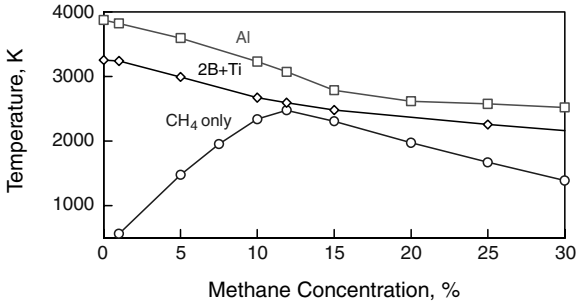

Fig. 1 Calculated combustion temperatures at a constant pressure of 6 atm for the $CH_4/N_2/O_2$ gas mixtures with a fixed O_2 concentration of 22.5% and varied concentration of CH_4 and with Al and 2B + Ti fuels. The concentrations of Al and 2B + Ti were selected to represent the stoichiometric oxidation reactions in the absence of methane as described by idealized reactions (see text).

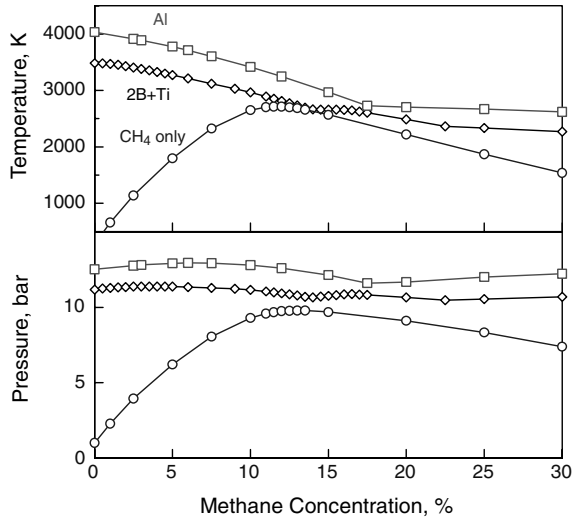

Fig. 2 Calculated adiabatic flame temperatures and pressures (in a constant 9.2 l volume) for the $CH_4/N_2/O_2$ gas mixtures with varied concentration of CH_4 and with Al and 2B + Ti fuels. The concentrations of Al and 2B + Ti were selected to represent the stoichiometric oxidation reactions in the absence of methane as described by idealized reactions (see text).

show that for the stoichiometric mixture, the adiabatic flame temperature is almost as high as that predicted for the same gas mixture with added 2B + Ti fuel.

Somewhat surprising, despite varying reaction temperatures, the pressures predicted in the constant-volume calculations do not seem to depend significantly on methane concentration when a metal fuel is used (cf. Fig. 2).

The calculations for metal combustion in gas mixtures with varied methane concentrations are shown in Figs. 3–5. For the purpose of these figures, the equivalence ratio was calculated based only on the amounts of metallic fuel and oxygen; methane was not considered. Again, the trends predicted for the constant-volume and constant-pressure calculations are similar. However, the predicted maximum flame temperatures are about 400 K higher for the constant-volume calculations (Fig. 4) than with the constant-pressure case (Fig. 3). The very high predicted temperatures substantially affect the species produced in the flame. In particular, the amounts of condensed metal oxide species are lower, which may result in substantial discrepancies with the experimental data.

The pressures of the constant-volume combustion calculations are shown in Fig. 5 as a function of the metal-oxygen-based equivalence ratio, which is proportional to the metal load for a constant oxygen concentration. It is interesting that the predicted pressures are nearly constant around the equivalence ratio 1, as well as that the maximum predicted pressures are nearly the same for calculations with different

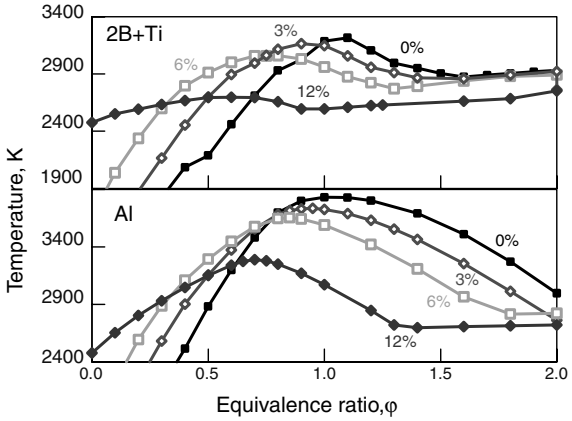

Fig. 3 Calculated flame temperatures at a constant pressure of 6 atm for the $CH_4/N_2/O_2$ gas mixtures with 0, 3, 6, and 12% of CH_4 (as curve labels show) and with different amounts of Al and 2B + Ti fuels. Note that the equivalence ratio in this plot is calculated based only on metal-oxygen reaction.

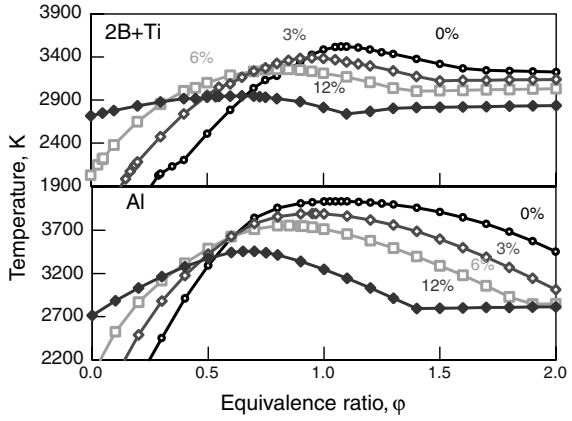

Fig. 4 Calculated adiabatic flame temperatures in a constant 9.2 l volume for the $CH_4/N_2/O_2$ gas mixtures with 0, 3, 6, and 12% of CH_4 (as curve labels show) and with different amounts of Al and 2B + Ti fuels. Note that the equivalence ratio in this plot is calculated based only on metal-oxygen reaction.

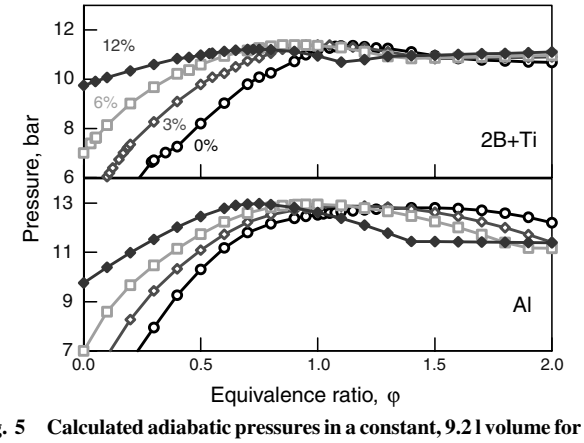

Fig. 5 Calculated adiabatic pressures in a constant, 9.2 l volume for the $CH_4/N_2/O_2$ gas mixtures 0, 3, 6, and 12% of CH_4 and with different amounts of Al and 2B + Ti fuels. Note that the equivalence ratio in this plot is calculated based only on metal-oxygen reaction.

methane concentrations. This is an alarming sign, indicating that if combustion in constant-volume explosion experiments indeed occurs in a way similar to that predicted by the thermodynamic equilibrium at a constant volume, the measured maximum pressures would not be changing at different experimental conditions and thus would not be useful as indicators of the combustion completeness. Fortunately, the measured pressures were found to depend significantly on both the methane concentration and the type of metallic fuel used.

Initial experiments showed that the pressures were substantially lower than those predicted by the constant-volume calculations. This implied that the flame temperatures were also substantially overpredicted. The significant difference in the calculated and experimental flame temperature in turn implies a great discrepancy between the combustion products predicted by constant-volume calculations and those produced in experiments. Note that a simple assumption that only a part of metal fuel participates in combustion cannot be used to resolve this problem successfully. It turns out that the fractions of metal fuel that need to react in the thermodynamic equilibrium calculations matching the experimental pressures are much lower than those observed to react experimentally, based on the analysis of the collected combustion products (discussed later, in the Results section). On the other hand, the constant-pressure calculations used a pressure from the low end of the experimental range and predicted a lower adiabatic flame temperature, which appeared to represent the experimental conditions better. Therefore, only the results of the preceding constant-pressure calculations performed at a pressure selected within the range observed experimentally were used for further selection of experimental conditions and for interpretation of the experimental data.

The results of calculations presented in Fig. 3 were used to select the concentrations (or respective mass loads) of each metal fuel corresponding to the peak adiabatic flame temperature for each gas composition. These mass loads shown in Table 1 were used in the experiments. Note that changes in the adiabatic flame temperatures in the vicinity of the peaks are weak, and so the experimental results should not be very sensitive to unavoidable small variations in the mass of powder injected into the vessel in the nominally identical experiments. Also shown in Table 1 are the respective adiabatic flame temperatures T_{ad} calculated for each specific gas mixture, as well as the molar amount of gaseous combustion products χ produced at T_{ad} for each case relative to the initial gas mixture. The coefficient χ includes all (permanent and transient) gaseous species at T_{ad}. This coefficient was later used to recover the flame temperatures from pressure measurements in the constant-volume explosion experiments. With the addition of methane, the value of χ grows, primarily because of production of such gas species as H_2 and CO.

The adiabatic flame temperatures predicted for Al are systematically higher than for 2B + Ti. This difference, however, may not represent a benefit in a practical application, considering that greater mass loads of Al were required for each calculation to achieve the maximum flame temperature for the same amount of gas mixture. In addition, the predicted adiabatic flame temperatures exceeding 3000 K can hardly be expected in experiments because of the significantly increased radiation heat losses. The results of the thermodynamic calculations can be used to better evaluate the effectiveness of different metallic fuels by calculating the heat release W per unit mass of metal that would be transferred to the internal energy of gaseous combustion products. This is the fraction of the combustion energy that would be used to create a pressure increase, whereas the rest of the energy will be absorbed by the condensed products and is of little practical interest.

Assuming that most of the combustion gases are diatomic so that their molar heat capacity can be roughly estimated as $C_V = 5/2R$, where R is the universal gas constant, the value of W can be calculated as

$$W = \frac{5}{2}\frac{R(T_{ad} - T_0)}{m}\mu \cdot \chi \tag{1}$$

where T_0 is room temperature and μ is the starting molar amount of gas in the combustion vessel. The assumption of diatomic gases is justified, because the preceding equilibrium calculations show that diatomic gas species (including CO, H_2, N_2, and others) make up the

Table 1 Results of thermodynamic equilibrium calculations, including: mass loads of metal fuels *m*, predicted to provide the maximum flame temperature for the constant-volume explosion experiments in a 9.2-liter vessel, initially at 1 atm; respective adiabatic flame temperatures T_{ad}, and change in the molar amount of gas χ present at T_{ad} relative to the starting gas mixture.

		Gas mixtures			
Fuel	Parameters	0.225 O_2, 0.775 N_2	0.225 O_2, 0.745 N_2, 0.030 CH_4	0.225 O_2, 0.715 N_2, 0.060 CH_4	0.225 O_2, 0.655 N_2, 0.120 CH_4
Al	m, g	2.89	2.79	2.64	2.17
	T_{ad}, K	3864	3733	3590	3290
	χ	0.86	0.91	0.96	1.05
2B + Ti	m, g	2.40	2.00	1.68	1.2
	T_{ad}, K	3217	3146	3025	2694
	χ	0.91	0.94	0.98	1.06

majority (about 90%) of the gas phase at T_{ad}. The value of μ, consistent with the data presented in Table 1, can be taken as $\mu = 0.3824$, to represent the experiments in a 9.2-liter vessel initially at 1 atm. The calculated values of W are shown in Fig. 6. These results indicate that per unit mass, the energy of combustion of 2B + Ti is more effectively transferred to heat the product gases than with Al. Note that this comparison is for the amounts of metal fuel selected to achieve the highest combustion temperature for each specific gas mixture. It should also be noted that this energy is produced exclusively by metal combustion only for the N_2/O_2 gas mixtures. For the $N_2/O_2/CH_4$ mixtures, the energy is released by combined reactions of oxidation of metal and CH_4.

Materials

Nanocomposite 2B + Ti powders were synthesized by ARM [9,10] using a Retsch PM 400-MA planetary mill. The mill was modified by the addition of an air conditioner to the milling chamber to achieve lower effective milling temperatures. The milling jars were equipped with wireless temperature sensors to monitor the process temperature. The starting materials were powders of amorphous boron (nominal size 0.7 μm, 98.5% pure, by SB Boron) and titanium (−325 mesh, 99.7% pure, by Atlantic Equipment Engineers). The same powders were mixed to prepare the blends (or mixtures) used in the comparison experiments. Additional experiments were performed with a spherical Al powder (nominal size of 1–5 μm, 99.9% pure, by Atlantic Equipment Engineers). This specific Al powder was selected based on our earlier constant-volume explosion experiments in which the highest burning rate was measured for this powder, compared with several other spherical Al powders and Al flakes [13]. Thus, the reference performance of Al was maximized to provide the most conservative assessment of possible benefits offered by the nanocomposite 2B + Ti powders.

The nanocomposite powders were prepared in this project using a sequence of two milling steps. In the first step, the powders were milled with a small amount of liquid process control agent (heptane) until the desired nanostructured refinement was achieved. In the second step, the amount of heptane was substantially increased and the resulting slurry was milled to minimize agglomeration and achieve the desired particle size distribution. Further details describing the synthesis methodology of the nanocomposite powders by mechanical milling are available elsewhere [9,10].

The particle size distributions for all powders used in this project were measured by low-angle laser light scattering using a Coulter LS 230 analyzer. The results of these measurements are presented in Fig. 7. The size distribution for the blend is clearly bimodal. This generally represents the sizes of the starting powders, with the boron being primarily responsible for the peak between 1 and 2 μm and titanium being primarily responsible for the peak around 33 μm. The size distribution for the nanocomposite powder repeats that of the blend for the fine-particle sizes indicating the presence of very fine, loose, boron particles. However, the right side of the size distribution clearly indicates the formation of new particles, which represent the targeted nanocomposite material. The size distribution for aluminum is generally narrower and the mean particle size (shown in Fig. 7) is somewhat finer.

The nanocomposite powders of 2B + Ti were also examined using a scanning electron microscope (SEM, LEO 1530). A typical SEM image obtained using backscattered electrons is presented in Fig. 8. The nanosized boron particles (dark) are embedded into a titanium matrix (light), producing a highly developed, reactive B-Ti interface. A few unattached boron particles are also visible in the image. X-ray-diffraction analysis of the nanocomposite powder showed no traces of the crystalline boride phases.

Experimental

Constant-volume explosion experiments were used to characterize the reactivity of the powders. This experimental technique is similar to that developed by the U.S. Bureau of Mines [11,12]. A schematic diagram of the apparatus is presented in Fig. 9; the experimental details are described elsewhere [8,13]. Before each

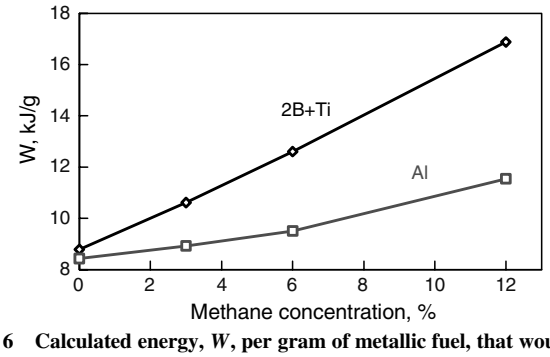

Fig. 6 Calculated energy, *W*, per gram of metallic fuel, that would be used to produce heated gaseous products of combustion in the $N_2/O_2/CH_4$ gas mixtures with metallic fuels added to achieve the maximum flame temperatures, according to Table 1.

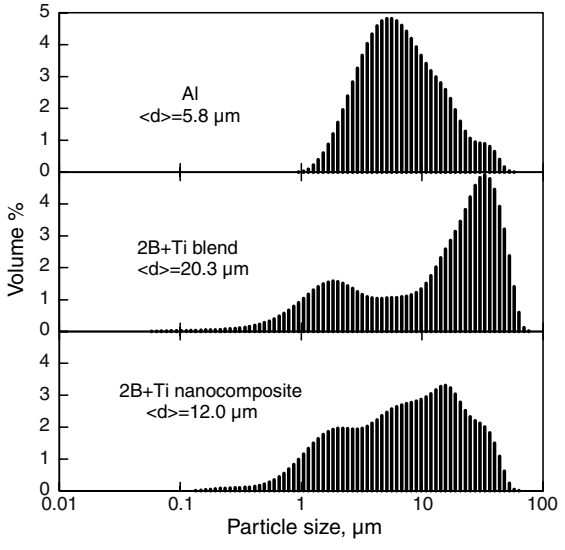

Fig. 7 Size distribution histograms for the powders used in experiments. The curve labels show the volume mean particle sizes.

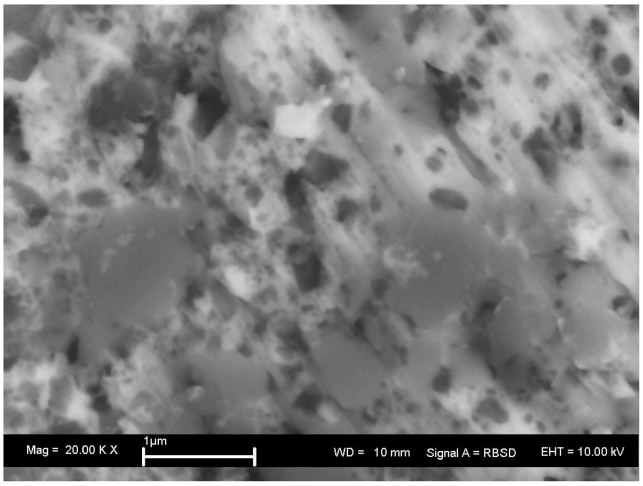

Fig. 8 A backscattered electron SEM image of the produced boron-titanium nanocomposite powder. Light and dark areas represent titanium and boron, respectively.

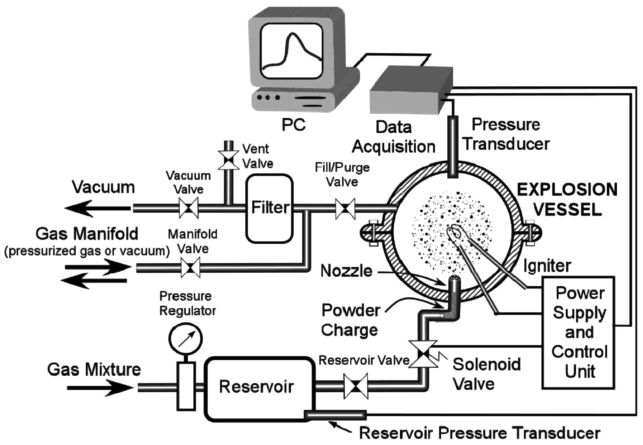

Fig. 9 Schematic diagram of the constant-volume explosion apparatus.

experiment, a powder charge with a mass as determined from Table 1 was placed in a pipe elbow under the nozzle, and the explosion vessel was closed and evacuated. For experiments with methane–air mixtures, the vessel was purged and filled with low-pressure oxygen. The high-pressure methane–nitrogen gas mixture carrying the aerosol into the vessel was prepared in a reservoir. This way, the ignition of the metal powder occurred only after the methane was mixed with oxygen. The reservoir was filled with the desired gas composition to a pressure of approximately 4 atm. The powder charge was introduced to the explosion vessel with a gas blast from the reservoir through a solenoid valve (cf. Fig. 9). The pressure in the reservoir tank was selected so that within the 0.2 s period over which the solenoid valve was open, the pressure in the explosion vessel reached 1 atm. Following a delay of 0.3 s, provided to reduce the turbulence in the explosion vessel, the igniter was activated. The igniter, an 8-mil (203.2-μm-diam) tungsten wire was heated up using an ac voltage selected to melt the wire within 60 ms, which limited the duration of the ignition energy input. The estimated total energy supplied to the igniter was 30 J. The pressure was measured using a transducer by Schaevitz Sensors and recorded using a Rapid Systems four-channel digital oscilloscope board. Simultaneously, the ignition pulse was recorded for time reference. The final pressure in the explosion vessel, reduced due to the consumption of oxygen, was recorded after the combustion was completed and after a delay of several minutes to allow the gas in the vessel to cool to room temperature. After the vessel pressure was brought to 1 atm, the vessel was opened, and the condensed products were collected for further analysis. Phase compositions of the combustion products were analyzed using x-ray diffraction.

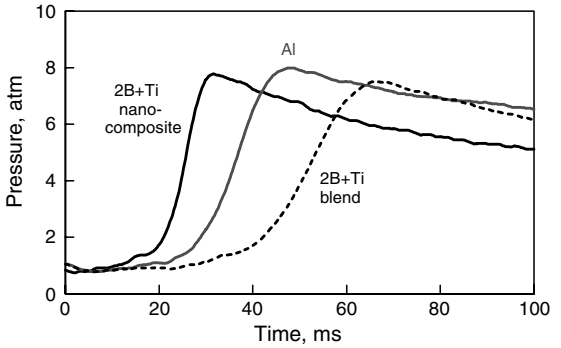

Fig. 10 Examples of pressure traces recorded in constant-volume experiments with different fuels. All traces shown are for the 0.225 O_2 + 0.715 N_2 + 0.06 CH_4 gas mixture. The fuel mass loads are shown in Table 1.

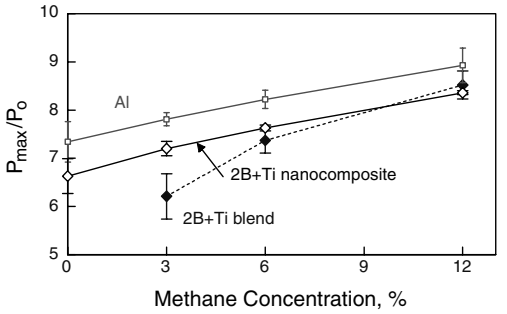

Fig. 11 Ratios of maximum pressure rise over initial pressure in the chamber measured for different metallic powders ignited in different $N_2/O_2/CH_4$ mixtures.

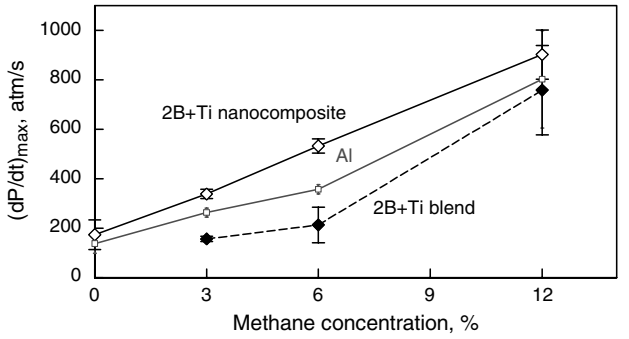

Fig. 12 Maximum rates of pressure rise measured for different metallic powders ignited in different $N_2/O_2/CH_4$ mixtures.

Results

At least three experiments were performed for each experimental condition (i.e., for each type of fuel and specific gas mixture). In cases in which a significant difference between identical runs was observed, the number of experiments was increased. Note that the $N_2/O_2/CH_4$ mixtures with 3% volumetric methane content could not be ignited by the hot-wire igniter when no metal fuel was present in the vessel. Also, no ignition could be achieved in experiments with powder blends 2B + Ti in the methane-free gas mixture. Finally, no ignition could be achieved in a limited number of experiments using only boron powder as a fuel.

Examples of the pressure traces for all materials for a selected gas composition are shown in Fig. 10. The ratios of the maximum observed pressure P_{max} to the initial gas pressure P_0 are plotted in Fig. 11 for different powders and different gas compositions. The maximum rates of pressure rise for all experiments are compared in Fig. 12. The error bars in both cases represent the standard deviations of experimental data for different gas-mixture/metal-fuel combinations.

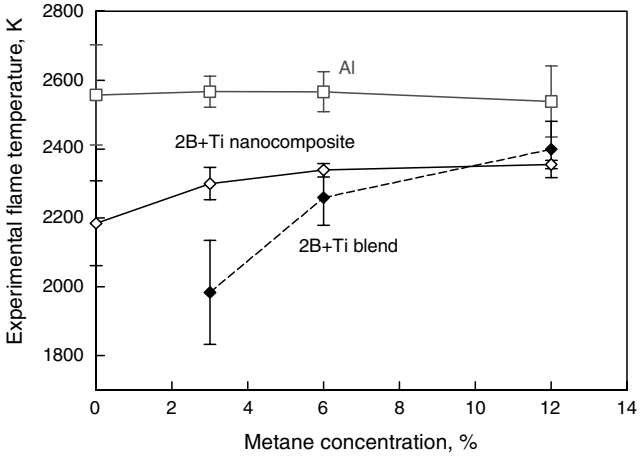

Fig. 13 Maximum experimental flame temperatures evaluated from the measured pressure traces for different metallic powders ignited in different $N_2/O_2/CH_4$ mixtures.

The pressure ratios shown in Fig. 11, commonly considered as indicators of the flame temperature [15,16], are consistently higher for Al, indicating that higher flame temperatures were achieved, as predicted by the thermodynamic equilibrium calculations (see Table 1). However, these ratios are also affected by the change in the number of moles of gas, as a result of oxygen consumption and production of gaseous suboxides. To obtain a better assessment of and comparison between the experimental flame temperatures, one needs to take into account the molar amount of gas in the vessel after the combustion reaction, which generally differs from the initial molar amount of gas. The coefficient χ quantifying this change was already introduced. The values of this coefficient shown in Table 1 were used to estimate the flame temperatures using the experimental pressure ratio P_{max}/P_0. Thus, the maximum experimental flame temperatures were estimated as

$$T_{max} = T_0 \frac{P_{max}}{P_0} \frac{1}{\chi} \tag{2}$$

The flame temperatures calculated according to Eq. (2) are shown in Fig. 13. It is interesting that the temperature obtained for the experiments using Al powder almost does not change as a function of methane concentration. It is also interesting that the flame temperature for 2B + Ti increases with added methane, indicating that not only the combustion rates (cf. Fig. 12), but also the combustion completeness, increased in wet environments.

The rates of pressure rise are usually considered to indicate the speed of flame propagation. The maximum rate of pressure rise (presented in Fig. 12) for each experiment is observed when the flame reaches the wall of the vessel [15,16]. The difference in the rates of pressure rise for different fuels, illustrated in Fig. 10, is representative of the overall observed trend in Fig. 12. The flame speeds were generally higher for the nanocomposite 2B + Ti powder followed by Al, with the lowest flame speeds observed for the 2B + Ti powder blends. However, the difference between different metallic fuels becomes comparable with the experimental data scatter when the concentration of CH_4 reaches 12%.

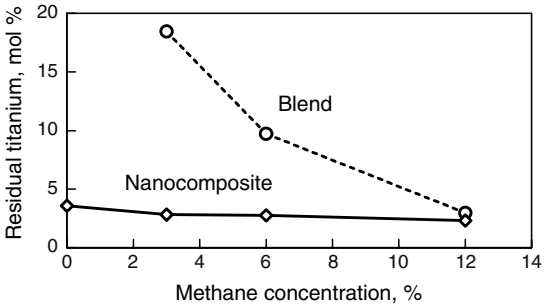

Fig. 14 Residual Ti present in the combustion products of 2B + Ti nanocomposite and blended powders for environments with different methane concentrations.

The combustion completeness was also evaluated using x-ray diffraction (XRD) of the condensed combustion products collected after the experiments. XRD was performed on a Phillips X'pert MRD powder diffractometer operated at 45 kV and 40 mA using Cu Kα radiation ($\lambda = 1.5438$ Å). The XRD patterns were processed using the General Structure Analysis System (GSAS) whole-pattern-fitting software package [17].

The primary phases identified in the combustion products of 2B + Ti were $B(OH)_3$, TiB_2, TiO_2 (both anatase and rutile), and Ti. Both boron and its anhydrous oxides are poorly crystalline and could not be clearly identified from XRD. It is also likely that the boron oxide formed in combustion ages in room air containing moisture, producing $B(OH)_3$. The most unambiguous assessment of the reaction completeness for 2B + Ti powders could be made by comparing the amounts of unreacted titanium for experiments with different samples ignited in different environments. The results of this analysis are presented in Fig. 14. It is clear that at lower methane concentrations, the reaction completeness for the nanocomposite powder is significantly better than for the powder blend. The difference in completeness nearly disappears at high methane concentrations.

XRD results were equally processed for the products collected after Al combustion experiments. The patterns showed the presence of large amounts of unreacted Al metal, varying in the range of 30 to more than 50 mol % for different gas environments. The experimental and computational patterns matched, satisfactorily considering products as a mixture of Al, δAl_2O_3, αAl_2O_3, and an amorphous or poorly crystalline phase. The amount of the amorphous or poorly crystalline phase was quantified using an internal standard, a predetermined amount of SiO_2 powder added to the samples before x-ray-diffraction patterns were collected. The results of quantitative analysis are presented in Table 2. The changes in the concentration of unreacted Al do not seem to follow the changes in the CH_4 concentration in the initial gas composition. Although more measurements would be required to further investigate the significance of this variation in the Al concentration, the presence of a substantial amount of unreacted metallic aluminum in the combustion products of aluminum powders was established.

Discussion

The thermodynamic calculations showed that despite the higher adiabatic flame temperatures predicted for Al, the gaseous

Table 2 Compositions of aluminum combustion products determined by whole pattern refinement of the x-ray-diffraction patterns for condensed products collected in different experiments. Concentrations of components are normalized per mole of aluminum. For the purpose of this estimate, the amorphous component was assumed to have Al_2O_3 composition as well.

	Condensed product composition, mole %			
Percentage of CH_4 in gas mixture	Al	δAl_2O_3	αAl_2O_3	Amorphous/poorly crystalline phase
0	53.9	17.9	1.1	27.0
3	27.4	22.5	2.5	47.6
6	59.3	14.6	4.9	21.2
12	34.5	20.2	5.6	39.8

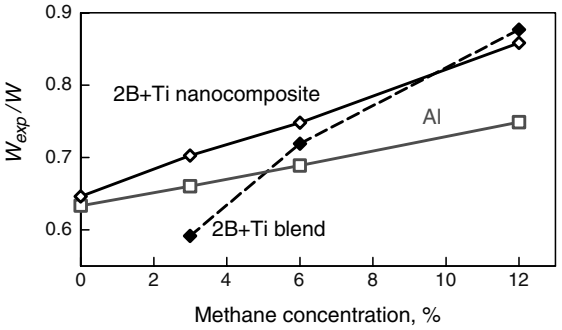

Fig. 15 Combustion efficiencies for different fuels combusting in difference $N_2/O_2/CH_4$ gas mixtures.

combustion products are expected to be heated more effectively when 2B + Ti fuels are used. Although both fuels are nearly equivalent for N_2/O_2 gas mixtures, a substantially better gas heating efficiency per unit mass of fuel is predicted for the boron-based fuel in wet environments. This result, illustrated in Fig. 6, is important for the selection of a metallic fuel optimized for a specific application.

The heat release predicted by thermodynamic calculations available for gas heating can now be compared with the experimental results. Specifically, modifying Eq. (1) by replacing the adiabatic flame temperature T_{ad} with the maximum flame temperature T_{max} evaluated from experimental data according to Eq. (2), the experimental value for the heat release W_{exp} per unit mass of the metallic fuel can be obtained. The ratio of W_{exp}/W can now be used as an indicator of the combustion efficiency for each fuel. These ratios for Al, 2B + Ti nanocomposite, and blended 2B + Ti powders are plotted in Fig. 15. The combustion efficiency is relatively low for the 2B + Ti blended powders at low methane concentrations, but it increases as the concentration of methane increases. This trend generally correlates with the combustion rates inferred for the powder blends from the rates of pressure rise presented in Fig. 12. The combustion efficiency is higher for the 2B + Ti nanocomposite powder than with Al for all environments tested. The comparison of combustion efficiencies based on the W_{exp}/W ratio is consistent with the XRD analysis of the combustion products. Again, this result seems to be in general agreement with the combustion-rate assessments, based on comparison of the maximum rates of pressure rise. However, although at the highest methane concentration of 12%, the measured combustion rates become close to one another for all materials, the efficiency of combustion for the nanocomposite 2B + Ti expressed through W_{exp}/W is similar to that of Al only in dry environments. The discrepancy between the efficiencies of 2B + Ti and Al becomes greater at higher methane concentrations. At the same time, the difference between the nanocomposite and blended powders of 2B + Ti becomes less and less noticeable as the methane concentration increases (cf. Figs. 14 and 15). The significant difference in the burn rates of blended and nanocomposite 2B + Ti powders for low methane concentrations (cf. Fig. 12) can be interpreted by considering the difference in the particle ignition mechanisms. It is suggested that for nanocomposite powders, the exothermic solid–solid reaction $2B + Ti \rightarrow TiB_2$ results in a temperature boost of nanocomposite particles, which accelerates the rates of ensuing oxidation reactions. Although the same solid–solid reaction could also occur in the blended powders, the observation that such powders could not be ignited in the absence of methane suggests that this reaction is practically negligible.

The high rates and combustion efficiencies observed for the boron-based fuels in wet environments indicate that the effect of the HOBO kinetic trap, which is often assumed to result in poor combustion completeness of boron in the presence of hydrogen, could not be detected in these experiments. In fact, the ratio of W_{exp}/W increased to almost 0.9 at increased methane concentrations, indicating that the combustion of 2B + Ti approached the conditions predicted by thermodynamic equilibrium. It is also interesting that the difference between the nanocomposite and blended 2B + Ti powders essentially disappeared at high methane concentration, when the overall combustion rate was substantially influenced by the methane–oxygen reaction.

Conclusions

The results of thermodynamic calculations for Al and 2B + Ti burning in $N_2/O_2/CH_4$ gas mixtures were interpreted to evaluate the portion of combustion energy used to produce heated gaseous products. This energy normalized per unit mass of metal fuel was found to be consistently higher for 2B + Ti than for Al for the entire range of gas mixtures considered, despite the higher adiabatic flame temperatures predicted for Al.

Constant-volume explosion experiments confirmed that the flame temperatures for Al in $N_2/O_2/CH_4$ gas mixtures are higher than those for both nanocomposite and blended powders of 2B + Ti. The combustion temperature for Al burning in different gas mixture remained nearly constant at about 2560 K. The combustion temperature for the nanocomposite 2B + Ti increased from about 2180 to 2370 K as the methane concentration increased from 0 to 12%. At high methane concentration, the combustion temperatures obtained for nanocomposite and blended 2B + Ti powders were nearly the same.

The bulk burn rates inferred from the rates of pressure rise were consistently higher for the nanocomposite 2B + Ti powder, followed by Al and then by the blended 2B + Ti powder. The difference in the burn rates became small when the concentration of methane increased to 12%.

The efficiency of combustion for all the fuels was assessed by comparing predicted and experimental portions of combustion energy per unit mass of metal fuel used to produce the heated gaseous products. Based on this assessment, nanocomposite boron-based fuels outperformed Al for all environments, with the difference increasing at higher methane concentrations. Nearly complete combustion was observed for both 2B + Ti fuels (nanocomposite and blended powders) at high methane concentration, when the highest rates of combustion were also observed. Thus, the effect of a kinetic trap associated with the formation of HOBO could not be detected.

Combustion of nanocomposite boron-based fuels is found to result in a more effective production of heated gas products for all environments considered. At low methane concentrations, the extended ignition delays characteristic of pure boron result in poor efficiencies or incomplete combustion for the blended powders. This problem is circumvented for the nanocomposite 2B + Ti powders, enabling rapid ignition in all environments because of the exothermic boron–titanium reaction. Thus, use of nanocomposite 2B + Ti powders enables one to achieve rapid and highly efficient combustion in both dry and wet gaseous environments.

Acknowledgments

This work was primarily supported by the Defense Threat Reduction Agency (William Wilson) with additional support from the Office of Naval Research (Judah Goldwasser).

References

[1] Yeh, C. L., and Kuo, K. K., "Ignition and Combustion of Boron Particles," *Progress in Energy and Combustion Science*, Vol. 22, No. 6, 1996, pp. 511–541. doi:10.1016/S0360-1285(96)00012-3

[2] Foelsche, R. O., Burton, R. L., and Krier, H., "Boron Particle Ignition and Combustion at 30–150 atm.," *Combustion and Flame*, Vol. 117, Nos. 1–2, 1999, pp. 32–58. doi:10.1016/S0010-2180(98)00080-7

[3] King, M. K., "Combustion of Boron Based Solid Propellants and Fuels," *Combustion of Boron-Based Solid Propellants and Solid Fuels*, edited by K. K. Kuo and R. Pein, CRC Press, Boca Raton, FL, 1993, pp. 1–79.

[4] Pasternack, L., "Gas-phase Modeling of Homogeneous Boron/Oxygen/Hydrogen/Carbon Combustion," *Combustion and Flame*, Vol. 90, Nos. 3–4, 1992, pp. 259–268. doi:10.1016/0010-2180(92)90087-6

[5] Yetter, R. A., Rabitz, H., Dryer, F. L., Brown, R. C., and Kolb, C. E., "Kinetics of High-Temperature B/O/H/C Chemistry," *Combustion and Flame*, Vol. 83, Nos. 1–2, 1991, pp. 43–62. doi:10.1016/0010-2180(91)90202-M

[6] Li, S. C., and Williams, F. A., "Ignition and Combustion of Boron Particles," *Combustion of Boron-Based Solid Propellants and Solid Fuels*, edited by K. K. Kuo and R. Pein, CRC Press, Boca Raton, FL, 1993, pp. 248–271.

[7] Dreizin, E. L., Keil, D. G., Felder, W., and Vicenzi, E. P., "Phase Changes in Boron Ignition and Combustion," *Combustion and Flame*, Vol. 119, No. 3, 1999, pp. 272–290. doi:10.1016/S0010-2180(99)00066-8

[8] Schoenitz, M., Dreizin, E. L., and Shtessel, E., "Constant Volume Explosion of Aerosols of Metallic Mechanical Alloys and Powder Blends," *Journal of Propulsion and Power*, Vol. 19, May–June 2003, pp. 405–412.

[9] Schoenitz, M., Ward, T. S., and Dreizin, E. L., "Fully Dense Nano-Composite Energetic Powders Prepared by Arrested Reactive Milling," *Proceedings of the Combustion Institute*, Vol. 30, No. 2, 2005, pp. 2071–2078. doi:10.1016/j.proci.2004.08.134

[10] Dreizin, E. L., and Schoenitz, M., "Nano-Composite Energetic Powders Prepared by Arrested Reactive Milling," U.S. Patent Application 20060053970, filed 12 Nov. 2004.Mar. 2006.

[11] Cashdollar, K. L., and Chatrathi, K., "Minimum Explosible Dust Concentrations Measured in 20-L and 1-M^3 Chambers," *Combustion Science and Technology*, Vol. 87, Nos. 1–6, 1993, pp. 157–171. doi:10.1080/00102209208947213

[12] Hertzberg, M., Zlochower, I. A., and Cashdollar, K. L., "Metal Dust Combustion: Explosion Limits, Pressures, and Temperatures," *Symposium (International) on Combustion*, Combustion Inst., Pittsburgh, PA, 1992, pp. 1827–1835.

[13] Eapen, B. Z., Hoffmann, V. K., Schoenitz, M., and Dreizin, E. L., "Combustion of Aerosolized Spherical Aluminum Powders and Flakes In Air," *Combustion Science and Technology*, Vol. 176, No. 7, 2004, pp. 1055–1069. doi:10.1080/00102200490426433

[14] Gordon, S., and McBride, B. J. "Computer Program for Calculation of Complex Chemical Equilibrium Compositions and Applications," NASA Reference Publication 1311, 1996.

[15] Glassman, I., *Combustion*, 3rd ed., Academic Press, San Diego, CA, 1996.

[16] Kuo, K. K., Principles of Combustion, Wiley Interscience, New York, 1986.

[17] Larson, A. C., and Von Dreele, R. B., "GSAS: General Structure Analysis System," Los Alamos National Lab., Rept. LAUR 86-748, Los Alamos, NM, 2000.

S. Son
Associate Editor